ELSEVIER

Chemical Geology 235 (2006) 105–123

CHEMICAL GEOLOGY
INCLUDING
ISOTOPE GEOSCIENCE

www.elsevier.com/locate/chemgeo

Oxygen diffusion in titanite: Lattice diffusion and fast-path diffusion in single crystals

X.Y. Zhang *, D.J. Cherniak, E.B. Watson

Department of Earth and Environmental Sciences Rensselaer Polytechnic Institute Troy, NY 12180, USA

Received 18 December 2005; received in revised form 20 June 2006; accepted 26 June 2006

Editor: P. Deines

Abstract

Oxygen diffusion in natural and synthetic single-crystal titanite was characterized under both dry and water-present conditions. For the dry experiments, pre-polished titanite samples were packed in ^{18}O-enriched quartz powder inside Ag–Pd capsules, along with a fayalite–magnetite–quartz (FMQ) buffer assemblage maintained physically separate by Ag–Pd strips. The sealed Ag–Pd capsules were themselves sealed inside evacuated silica glass tubes and run at 700–1050 °C and atmospheric pressure for durations ranging from 1 h to several weeks. The hydrothermal experiments were conducted by encapsulating polished titanite crystals with ^{18}O enriched water and running at 700–900 °C and 10–160 MPa in standard cold-seal pressure vessels for durations of 1 day to several weeks. Diffusive uptake profiles of ^{18}O were measured in all cases by nuclear reaction analysis (NRA) using the ^{18}O (p,α) ^{15}N reaction.

For the experiments on natural crystals, under both dry and hydrothermal conditions, two mechanisms could be recognized as responsible for oxygen diffusion. The diffusion profiles showed two segments: a steep one close to the initial surface attributed to self diffusion in the titanite lattice; and a "tail" reaching deep into the sample attributable to diffusion in a "fast path" such as planar defects or pipes. For the experiments on synthetic crystals, lattice diffusion only is apparent in crystals with euhedral morphology, while both mechanisms operate in crystals lacking euhedral morphology.

For the dry experiments, the following Arrhenius relation was obtained:

$$D_{\text{dry lattice}} = 3.03 \times 10^{-8} \exp(-276 \pm 16 \text{kJmol}^{-1}/\text{RT}) \text{m}^2/\text{s}$$

Under wet conditions at P_{H_2O}=100 MPa, Oxygen diffusion conforms to the following Arrehenius relation:

$$D_{\text{wet lattice}} = 2.05 \times 10^{-12} \exp(-180 \pm 39 \text{kJmol}^{-1}/\text{RT}) \text{m}^2/\text{s}$$

Diffusive anisotropy was explored only at hydrothermal conditions, with little evidence of diffusive anisotropy observed.

Oxygen diffusivity shows no dependence on water pressure 800 °C (P_{H_2O}=10–160 MPa) or 880 °C (P_{H_2O}=10–100 MPa).

However, like many other silicates, titanite shows a lower activation energy for oxygen diffusion in the presence of H_2O than under dry conditions; therefore the difference between the "dry" and "wet" diffusivities increases as temperature decreases below the range of this study. For example, at 500 °C, dry diffusion is almost 2.5 orders of magnitude slower than wet diffusion. Accordingly, the retentivity of oxygen isotope signatures will be quite different between dry and wet systems at geologically interesting conditions. For most cases, wet diffusion results may be the appropriate choice for modeling natural systems.

Keywords: Titanite; Oxygen diffusion; Fast-path diffusion; Nuclear reaction analysis

* Corresponding author. Department of Geosciences, The University of Arizona Tucson, AZ 85721, USA. Fax: +1 520 621 2672.
E-mail address: zhangxy@email.arizona.edu (X.Y. Zhang).

0009-2541/$ - see front matter © 2006 Elsevier B.V. All rights reserved.
doi:10.1016/j.chemgeo.2006.06.005

1. Introduction

Titanite is a common accessory phase in igneous, metamorphic, and hydrothermal rocks, and also occurs as an authigenic phase in sedimentary rocks (Yau et al., 1987; Kowallis et al., 1997). Since it is relatively insoluble and tends to concentrate certain radioactive elements (i.e., U, Th) and important trace elements (e.g., REE), it is very important in geochemistry and geochronology (e.g., Frost et al., 2001). As a key U–Pb geochronometer, its importance is second perhaps only to zircon. U–Th–Pb dating of titanite and other accessory minerals (i.e. zircon, monazite) can usually indicate the time of the mineral-forming event, such as igneous crystallization, eruption, metamorphic peak, or hydrothermal event. Crystals with multistage growth histories may date more than one event. The oxygen isotopes in these accessory minerals, including titanite, may provide additional thermal information, e.g., equilibrium peak temperature of the events, cooling rate, and possible source of host rock. Coupling the above two sets of analysis (i.e., U–Th–Pb systems and oxygen isotope ratios) can provide more powerful tools for geologists to decipher additional complexities of the *P–T–t* history of the rock. When an accessory phase used in dating is the only mineral surviving a thermal event, oxygen isotopes may provide unique insight into thermal history, provided the original oxygen isotope ratios were not reset through diffusion.

Over the past 15 years, the development of in situ oxygen isotope measurement technology has made microanalysis of single crystals possible (Elsenheimer and Valley, 1991, 1992; Wiechert and Hoefs, 1995; Wiechert et al., 2002).

Zircon is the first candidate for which oxygen isotope composition has been linked with U–Pb ages as a tool to "see through" metamorphism and decipher complex igneous and metamorphic histories (Valley et al., 1994; Wilde et al., 2001; Mojzsis et al., 2001; Peck et al., 2001). Interpretation of these findings is also aided by the existence of laboratory measurements of both oxygen (Watson and Cherniak, 1997) and Pb (Cherniak and Watson, 2001) diffusivities in zircon. Titanite might be used in a similar manner, if its oxygen isotope characteristics can be linked with its recorded age, or subsequent thermal events. For this reason, detailed knowledge of oxygen diffusion in titanite is essential, as is assessment of its diffusion rate with respect to that for Pb isotopes.

Meanwhile, the empirical calibration of oxygen isotope fractionation for mineral pairs including titanite, is also available (King et al., 2001). Whether these calibrations can be employed as geothermometers also depends on whether the system remains closed with respect to oxygen isotopes, and thus on the oxygen diffusion systematics. Furthermore, as in situ oxygen isotope measurement techniques become more routine, it is increasingly likely that oxygen isotope zoning and other non-uniform textures will be discovered. Interpreting these fine-scale textures and extracting information from them cannot be realized without a better understanding of oxygen diffusion.

Oxygen diffusivities have been determined for a number of minerals (for a thorough review, see Cole and Chakraborty, 2001) including feldspars (Giletti et al., 1978; Derdau et al., 1998), garnet (Coghlan, 1990), quartz (Dennis, 1984; Gilletti and Yund, 1984; Farver and Yund, 1991a), diopside (Farver, 1989; Pacaud et al., 1999), calcite (Farver, 1994), amphiboles (Farver and Giletti, 1989), biotite, muscovite and phologopite micas (Fortier and Giletti, 1991), magnetite (Giletti and Hess, 1988), rutile (Moore et al., 1998), zircon (Watson and Cherniak, 1997), and monazite (Cherniak et al., 2004). At present, the only data for titanite are those of Morishita et al. (1996) for 700–900 °C, 100 MPa water pressure conditions. For the above reasons, we undertook a comprehensive experimental investigation to measure oxygen diffusion coefficients in titanite single crystals, using both natural crystals from different localities and synthetic crystals grown for this purpose. Experiments were run under both FMQ-buffered dry conditions and water-present (wet) conditions (near the Ni–NiO buffer). Results and geochemical implications of the experiments are discussed in detail in later sections of the paper.

2. Experiments and analysis

2.1. Experiment preparation

We used three natural crystals from different localities and one synthetic titanite for the experiments; compositions are listed in Table 1. To simplify the discussion, the natural titanite crystals were named crystal 1, crystal 2 and crystal 3. Crystal 1 is from Harts Ranges, NT, Australia. It is a clear, yellowish green crystal, 2 cm × 3 cm × 0.8 cm in size, with local microinclusions. Crystal 2 specimens are ~1 cm clear, green crystals with good natural growth faces from Capelinha, Minas Gerais, Brazil. Crystal 3 specimens are commercially cut, faceted and polished green gems with sizes of 2.5 mm or 3 mm, from Africa. The synthetic titanite specimens used for the experiments are ~1 mm and purplish-gray in color, some with good growth faces (for dry experiments, they are obvious single crystals with euhedral morphology) and some without (the crystals used for the wet experiments lack euhedral morphology). These crystals were synthesized in a piston-

Table 1
Composition of titanite used in the experiments (wt.%)

	Crystal 1	Crystal 2	Crystal 3	Synthetic
CaO	28.70	28.26	28.89	28.82
TiO_2	37.39	36.14	37.47	39.07
SiO_2	31.14	31.10	31.76	30.94
F	0.44	0.43	0	0.65
Al_2O_3	1.41	1.24	1.08	0.32
FeO[a]	0.24	0.51	0.61	0.20
MnO	0.02	0.03	0.06	0.006
MgO	0.004	0.004	0.006	0.50
K_2O	N.A.	0.024	0.009	0.000
Na_2O	N.A.	0.001	0.004	0.002
Total	98.90	97.31	99.89	99.86

Values are average of several electron-microprobe analyses.
[a] The total Fe was reported as FeO without determining its oxidation state.

cylinder apparatus from an oxide mixture of titanite composition, in a HF solution with excess SiO_2.

Crystal 1 was cut into ~1-mm-thick wafers perpendicular to axis *c* using a low-speed diamond saw, and polished using a series of alumina powers down to 0.3 μm size grit. These wafers were then cut into 1.5-mm squares. For crystal 2, some pieces were cut to preserve one of the natural growth faces of (110), (010) or (100) and others were cut and polished in the same way as crystal 1. For specimens of crystal 3, the pointed tips of the faceted crystals were cut off so that the biggest polished face could sit flat. Synthesized crystals were polished in a way to obtain the biggest possible polished surface.

The slabs selected for the experiments were clear, with no cracks or visible inclusions. Prior to the diffusion experiments, the slabs were pre-annealed in gold capsules at 950 °C for 70–90 h with fO_2 at the FMQ buffer. The purpose of the pre-annealing was to heal possible surface damage produced during the cutting and polishing processes and to equilibrate the crystals at FMQ-buffered conditions. The gold capsule was welded at one end and placed in a silica glass tube along with the oxygen buffer. The tube was then sealed under vacuum. The buffer was separated from the gold capsule with several small pieces of the silica glass. The upper end of the gold capsule was crimped, permitting oxygen gas communication between the titanite slabs and the buffer during the pre annealing step (Fig. 1A). The natural titanites retained their original yellowish-green color after pre-annealing, but the synthesized crystals lost their color. There is no difference between the diffusion profiles measured from natural growth faces and polished surfaces (see discussion in Results), which means that the pre-annealing removed any near surface defects caused by cold working (cutting and/or polishing), if such defects existed at all.

For the dry diffusion experiments, ^{18}O-enriched quartz (SiO_2) powder was used as the diffusion source. The powder was produced by reacting Si powder with ^{18}O enriched H_2O (with $^{18}O > 95$ at.% of total O) in a closed, noble-metal capsule at 800 °C, 120 MPa for 3–4 days. Hydrothermal diffusion experiments involved the use of ^{18}O water (with $^{18}O > 95$ at.% of total O) as the diffusion source.

2.2. Experimental techniques and strategy

2.2.1. Dry experiments at FMQ buffered conditions

A double container for the dry diffusion experiments was made in two steps: fabrication of the Ag–Pd capsule and sealing the Ag–Pd capsule in a silica glass tube under vacuum. The 3 mm diameter Ag–Pd capsules were partitioned into two chambers using Ag–Pd strips; the FMQ buffer was in the bottom chamber and the pre-annealed titanite slab was packed in the diffusant source ($Si^{18}O_2$ powder) in the upper chamber. Both ends of the Ag–Pd capsule were welded. The reason for this configuration is that the walls of the silica glass capsule can exchange oxygen with the diffusant source and thus may dilute the ^{18}O source if there is contact between the glass walls and $^{18}O_2$ vapor. The oxygen cannot escape readily from the sealed Ag–Pd capsule, but the sample is in communication with the buffer sharing the metal capsule. The exterior silica glass capsule serves to prevent the oxidation of the Ag–Pd capsule (Fig. 1B).

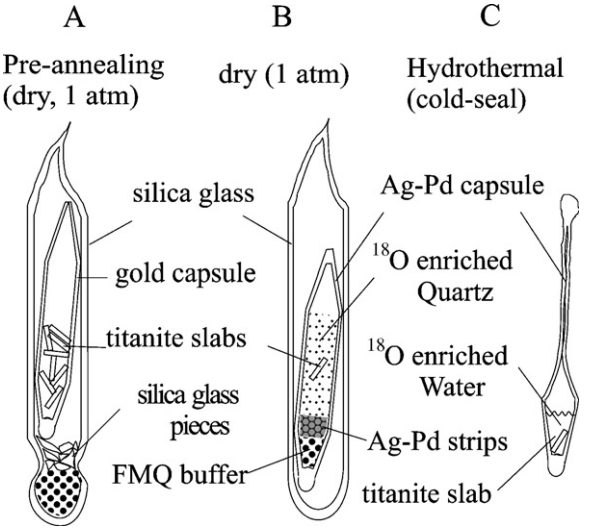

Fig. 1. Schematic configuration of the pre-annealing capsule (A), the dry-experiment capsule (B) and wet-experiment capsule (C) used to investigate ^{18}O diffusion in titanite. See text for discussion.

The sealed capsules were annealed in 1 atm vertical tube furnaces at temperatures ranging from 700 to 1050 °C for times of 1 h to 41 days. The temperatures were monitored by type K (chromel-alumel) thermocouples believed to be accurate within ±3 °C. Furnaces were preheated to the run temperature before inserting the sample capsules. The heat-up and quenching time was negligible relative to experiment durations. The quenching of dry experimental capsules, as well as later hydrothermal capsules, was achieved simply by removing the capsules from the furnaces and allowing them to cool naturally in the air. The run products were recovered from the diffusant source, then ultrasonically cleaned first in distilled water, then in ethanol, and saved for analysis.

Dry experiments include three temperature series. The comprehensive series is on crystal 1 from 700 to 1050 °C (total of 21 experiments, including a time series of 3 experiments at 900 °C). The other two temperature series are on crystal 2 from 750 to 1050 °C (5 experiments) and on the synthetic crystals, also from 750 to 1050 °C (4 experiments).

2.2.2. Hydrothermal experiments

Capsules for the hydrothermal experiments differed from those for 1 atm runs in that no buffer assemblage was added; the vessel itself maintained a buffer condition close to Ni–NiO during the runs, which is only slightly higher than the FMQ buffer. A few microliters of ^{18}O-enriched water and a piece of polished titanite slab were sealed in Ag–Pd or Au capsules (see Fig. 1C). The sealed capsules were run in Stellite or René 41 cold seal pressure vessels at temperatures ranging from 700 to 900 °C for times of a few days to about 2 months. Pressures were monitored by Bourdon-type gauges, with pressure accuracy within ~5 MPa. As in the 1 atm experiments, the uncertainty in temperature was ±3 °C.

The hydrothermal runs covered isobaric series and isothermal series. The main isobaric series consisted of

Table 2
Oxygen diffusion in titanite at dry conditions

Run no.	Crystal	Time (s)	T (°C)	log$D_{lattice}$ (m^2/s)	+/− (1σ)	log$D_{fastpath}$ (m^2/s)	+/− (1σ)
Dry experiments on natural crystals normal to (001)							
sph1	No. 1	8.640E+04	900	−19.70	0.15	−15.61	0.13
sph2	No. 1	2.340E+04	950	−19.21	0.09	−15.19	0.12
sph3	No. 1	3.480E+05	850	−20.76	0.11	−16.57	0.08
sph4	No. 1	7.260E+03	1000	−19.45	0.24	−14.62	0.21
sph5	No. 1	3.600E+03	1050	−19.36	0.29	−14.31	0.23
sph7	No. 1	1.814E+06	749	−21.65	0.24	−17.72	0.20
sph8	No. 1	4.838E+06	697	−22.43	0.47	−18.24	0.14
sph10	No. 1	8.929E+05	798	−20.98	0.09	−17.26	0.09
sph11	No. 1	2.382E+04	950	−19.28	0.10	−14.97	0.11
sph12	No. 1	3.240E+04	901	−19.61	0.20	−15.12	0.17
sph13	No. 1	3.024E+06	752	−21.04	0.30	−16.57	0.19
sph14	No. 1	7.200E+03	1000	−19.16	0.28	−14.09	0.17
sph15	No. 1	3.600E+03	1049	−18.91	0.25	−13.93	0.24
sph16	No. 1	4.838E+06	698	−22.04	0.08	−17.07	0.07
sph17	No. 1	1.210E+06	801	−21.11	0.12	−16.70	0.09
sph18	No. 1	3.492E+05	901	−19.31	0.30	−14.51	0.14
sph19	No. 1	2.333E+06	801	−21.78	0.18	−16.68	0.15
sph20	No. 1	3.600E+03	1049	−18.88	0.19	−13.88	0.16
sph21	No. 1	7.440E+03	999	−18.84	0.30	−14.14	0.32
sph22	No. 2	8.640E+04	900	−19.64	0.29	−14.89	0.19
sph23	No. 2	2.340E+04	950	−19.72	0.31	−14.84	0.21
sph24	No. 2	5.400E+03	1000	−18.48	0.07	−13.99	0.04
sph26	No. 2	3.600E+03	1050	−18.47	0.07	−13.32	0.05
sph36	No. 2	3.542E+06	751	−21.86	0.16	−18.35	0.14
Dry experiments on synthesized crystal normal to arbitrary direction							
sph28[a]	synthesized	1.728E+05	1054	−18.22	0.11		
sph31[a]	synthesized	6.091E+05	951	−19.07	0.15		
sph37[a]	synthesized	3.542E+06	751	−21.20	0.31		
sph39[a]	synthesized	1.988E+06	852	−20.84	0.30		

[a] Diffusion profiles have no "tail". There is no fast-path diffusion, only lattice diffusion occurs.

Table 3
Oxygen diffusion in titanite at hydrothermal conditions

Run no.	Crystal	Time (s)	T (°C)	P_{water} (MPa)	log$D_{lattice}$ (m^2/s)	+/− (1σ)	log$D_{fast\text{-}path}$ (m^2/s)	+/− (1σ)
Wet experiments on natural crystals normal to (001),100 MPa water pressure								
sphcs01	No. 2	9.720E+04	851	100	−20.14	0.30	−17.85	0.19
sphcs02	No. 2	3.456E+05	850	100	−19.98	0.22	−17.18	0.25
sphcs03	No. 2	1.210E+06	851	100	−20.31	0.15	−17.53	0.16
sphcs04	No. 2	3.456E+05	801	100	−19.84	0.31	a	
sphcs05	No. 2	8.640E+04	900	100	−19.85	0.15	a	
sphcs06	No. 2	2.437E+06	751	100	−21.08	0.31	a	
sphcs07	No. 2	5.018E+06	700	100	−21.07	0.23	−17.50	0.18
sphcs08	No. 2	4.320E+05	801	100	−20.08	0.19	−16.97	0.16
sphcs09	No. 2	4.493E+06	700	100	−21.55	0.33	−18.37	0.21
sphcs10	No. 2	3.456E+05	880	100	−19.65	0.30	−16.43	0.32
sphcs11	No. 2	2.592E+05	880	100	−19.87	0.24	−16.31	0.25
sphcs12	No. 2	1.555E+06	800	100	−20.73	0.12	a	
sphcs13	No. 2	4.486E+06	750	100	−21.21	0.29	−17.92	0.15
sphcs14	No. 2	4.126E+06	700	100	−21.57	0.24	−18.60	0.18
sphcs25	No. 2	8.652E+04	900	100	−19.89	0.28	a	
sphcs26	No. 2	4.234E+06	750	100	−20.64	0.22	−17.71	0.17
Wet experiments on natural crystals normal to (100),100 MPa water pressure								
sphcs15	No. 2	3.528E+05	880	100	−19.71[e]	0.11	b	
sphcs16	No. 2	5.185E+05	881	100	−19.94	0.16	a	
sphcs17	No. 2	1.210E+06	800	100	−20.85	0.36	−18.37	0.16
sphcs21	No. 2	4.234E+06	700	100	−21.02	0.14	−16.85	0.18
Wet experiments on natural crystals normal to (110),100 MPa water pressure								
sphcs18	No. 2	4.320E+05	880	100	−20.13	0.19	−16.57	0.13
sphcs19	No. 2	1.469E+06	802	100	−20.53	0.24	c	
sphcs24	No. 2	4.666E+06	700	100	−21.45	0.32	c	
Wet experiments on different natural crystals 880 °C, normal to (001) different P water								
sphcs10	No. 2	3.456E+05	880	100	−19.65	0.30	−16.43	0.32
sphcs11	No. 2	2.592E+05	880	100	−19.87	0.24	−16.31	0.25
sphcs27	No. 2	2.592E+05	880	70	−20.37	0.30	a	
sphcs41	No. 2	2.592E+05	880	40	−19.50	0.12	a	
sphcs59	No. 2	4.320E+05	881	10	−19.46	0.18	−14.96	0.36
sphcs28	No. 3	2.592E+05	880	70	−20.10	0.23	a	
sphcs29	No. 3	2.612E+05	880	40	−20.19	0.26	−17.79	0.35
sphcs46	No. 3	2.593E+05	879	100	−19.90	0.14	a	
Wet experiments on different natural crystals 800 °C, normal to (001) different P water								
sphcs04	No. 2	3.456E+05	801	100	−19.84	0.35	a	
sphcs08	No. 2	4.320E+05	801	100	−20.08	0.21	−16.97	0.34
sphcs12	No. 2	1.555E+06	800	100	−20.73	0.15	a	
sphcs32	No. 2	1.555E+06	800	70	−20.09[e]	0.09	b	
sphcs39	No. 2	1.555E+06	800	40	−20.27[e]	0.16	b	
sphcs43	No. 2	1.555E+06	801	160	−20.68	0.23	−18.00	0.25
sphcs48	No. 2	1.556E+06	799	130	−20.02	0.13	a	
sphcs55	No. 2	1.642E+06	800	70	−20.35	0.34	c	
sphcs57	No. 2	1.555E+06	799	40	−20.75	0.29	c	
sphcs60	No. 2	1.728E+06	800	10	−20.81	0.33	−17.01	0.30
sphcs31	No. 3	1.555E+06	800	70	−19.51[e]	0.31	b	
sphcs37	No. 3	1.555E+06	800	100	−20.66[e]	0.26	b	
sphcs38	No. 3	1.555E+06	800	40	−20.20	0.20	−16.82	0.25
sphcs42	No. 3	1.555E+06	800	10	−19.16[e]	0.19	b	
sphcs49	No. 3	1.642E+06	800	130	−19.69	0.16	a	
sphcs50	No. 3	1.642E+06	801	100	−20.40	0.32	c	
sphcs51	No. 3	1.555E+06	800	160	−21.03	0.19	a	

(continued on next page)

Table 3 (*continued*)

Run no.	Crystal	Time (s)	T (°C)	P_{water} (MPa)	log$D_{lattice}$ (m^2/s)	+/− (1σ)	log$D_{fast\text{-}path}$ (m^2/s)	+/− (1σ)
sphcs54	No. 3	1.642E+06	800	70	−19.78	0.23	c	
sphcs56	No. 3	1.555E+06	799	40	−19.65[e]	0.10	b	
sphcs61	No. 3	1.728E+06	800	10	−19.56	0.18	−16.24	0.29
Wet experiments on synthesized crystals normal to arbitrary direction								
Sphcs62	synthesized	1.728+E05	880	100	−19.70	0.09	−16.51	0.20
Sphcs63	synthesized	2.077+E06	800	100	−21.08	0.16	−16.05	0.15
Sphcs64	synthesized	4.234+E06	700	100	−21.07	0.21	−16.94	0.23

(a) Tail present, but too small to evaluate fast-path diffusivity. (b) Diffusion fields of adjacent fast-paths are overlapped — "type A" kinetics. (c) Medium-size tail but no obvious separation point; fast-diffusion paths partially overlap — intermediate type between type A and B kinetics. (d) Large tail but no obvious separation point; diffusion fields of adjacent fast-paths partially overlapped — intermediate type between type A and B kinetics. (e) Diffusivities show a simple error function fit, but fast apparent diffusivities are obtained.

runs for diffusion perpendicular to (001), with temperatures from 700 to 900 °C and pressure 100 MPa. Two other isobaric series, for diffusion perpendicular to (110) and (100), respectively, were run under conditions of temperatures from 700 to 880 °C and pressure 100 MPa to explore the possible anisotropy of oxygen diffusion in titanite. Ultimately, no anisotropy was evident. Two isothermal series of 800 °C and 880 °C were conducted at pressure ranges of 10–160 MPa and 10–100 MPa using crystal 2 with diffusion perpendicular to (001), and also with crystal 3 for an arbitrary diffusion direction to explore whether differing trace element composition might affect oxygen diffusion in titanite. In addition, a time series was conducted at 850 °C and 100 MPa to make sure that the diffusivities measured are not run-duration dependent.

As with the 1 atm experiments, the heating-up and quench time are negligible compared to the relatively long experimental annealing durations. The run conditions for both "dry" and "wet" experiments and the resulting diffusivities are listed in Tables 2 and 3, respectively.

2.3. Analytical methods and data reduction

2.3.1. Nuclear reaction analysis (NRA)

The oxygen concentration profiles were measured using the nuclear reaction ^{18}O (p,α) ^{15}N, which has been used to characterize diffusion profiles in a number of previous studies of oxygen diffusion in solids. Some previous workers used a beam of monoenergetic protons (H^+), with incident energies ranging from 470 to 825 KeV (Choudhury et al., 1965; Robin et al., 1973; Jaoul et al., 1980; Reddy and Cooper, 1982; Jaoul et al., 1983; Gerard and Jaoul, 1989; Ryerson et al., 1989); other researchers have used 1.65 MeV H_2^+ as the incident beam (Ryerson et al., 1989; Cherniak, 1990; Moore et al., 1998; Cherniak et al., 2004).The analyses in this study were performed at the 4.5 MeV Dynamitron accelerator facility in the Ion Beam Laboratory at State University of New York at Albany. 1.65 MeV H_2^+ was used as incident beam. The H_2^+ molecule dissociates near the crystal surface into two 825 KeV H^+ ions; it was found in earlier studies of oxygen diffusion in olivine that the NRA spectra of samples analyzed with both primary H_2^+ and H^+ beams were identical within analytical uncertainty (Ryerson et al., 1989; Cherniak, 1990). An advantage of the H_2^+ beam over the H^+ beam is that it is more stable and can be more easily focused into a smaller beam spot (Ryerson et al., 1989; Cherniak, 1990), a critical factor when dealing with small experimental samples. In most cases, the beam spot was ~1 mm^2. Most samples exceeded this size, but many cold seal run products were significantly smaller because the slabs were broken during the high pressure run or during depressurization and sample recovery. To measure the submillimeter samples, they were mounted in small epoxy disks for easier handling, and slits were used to reduce the beam spot size. The epoxy also contributed negligibly to the detected α signal due to the reaction with ^{18}O in cases where the beam spot was slightly larger than the sample and sharper focus could not be achieved.

The essence of the ^{18}O (p,α) ^{15}N method is that H^+ ions penetrate the crystal, react with ^{18}O nuclei in the sample, and produce α particles of specific energy as products of the nuclear reaction. The H^+ ions lose energy (at a known rate) as they penetrate the crystal prior to reacting with ^{18}O nuclei, and the resulting α particles generated at different depths have different energies. These α particles also lose energy (also at a known rate) traveling back out of the crystal. The NRA spectrum of α particle counts vs. energy (i.e. channel) is therefore a collection of α particles originating from different depths in the material. Since the α particle yield at specific energy channel is directly proportional to the ^{18}O concentration, and the α energy can be correlated with a specific depth given knowledge of energy loss rates of ingoing protons and outgoing α particles in the material, the concentration profile of ^{18}O

can be derived from the NRA spectra (Cherniak, 1990). Fig. 2A is a typical NRA spectrum. Typical ^{18}O concentration profiles are shown in Fig. 2B and C.

2.3.2. Diffusion coefficient reduction

All the diffusion experiments are designed to meet the condition that the titanite resides in an infinite ^{18}O-enriched reservoir and the uptake of the ^{18}O in the near surface of the crystal does not affect the ^{18}O concentration of the reservoir. Accordingly, the relevant boundary conditions are one dimensional diffusion into a planar surface with constant surface concentration. The diffusion profile will conform to a complementary error function solution if lattice diffusion only controls the diffusion behavior. However, two types of diffusion profiles were immediately recognized. One is a simple profile which conforms to a simple error function solution. The other kind is a "tailed" profile which consists of two segments: a near-surface part and a deeper penetrating "tail." These two diffusion profile types are classified by their appearance. These diffusion profiles can also be understood as resulting from two diffusion pathways: lattice diffusion and fast-path diffusion, either appearing as a simple diffusion profile or a composite profile showing both lattice diffusion and fast-path diffusion. However, the two groups of diffusion profiles classified by appearance and by mechanism are not necessarily related one to one. All lattice diffusion profiles under experimental boundary conditions are simple error function profiles, but not all simple profiles are lattice diffusion profiles, since some composite profiles can appear as simple profiles. Further explanation of these observations can be found in Section 2.3.2.2.

2.3.2.1. Lattice diffusion profiles. The simple diffusion profiles fit the solution of Fick's second law for diffusive transport into a semi-infinite medium through a planar surface held at constant surface concentration (Crank, 1967):

$$C(x) = C_0(1-\mathrm{erf}(\frac{x}{\sqrt{4Dt}})) \quad (1)$$

where C is the concentration of ^{18}O in the sample at some distance x from the surface, C_0 is the concentration of ^{18}O at the surface, D is the diffusion coefficient and t is the experiment duration. The fit can be done either by the non-linear fitting tool available in programs like Origin© or by conventional linear fitting of $\mathrm{erf}^{-1}(1-C/C_0)$ versus x, where the slope of the linear regression is $(4Dt)^{-1/2}$.

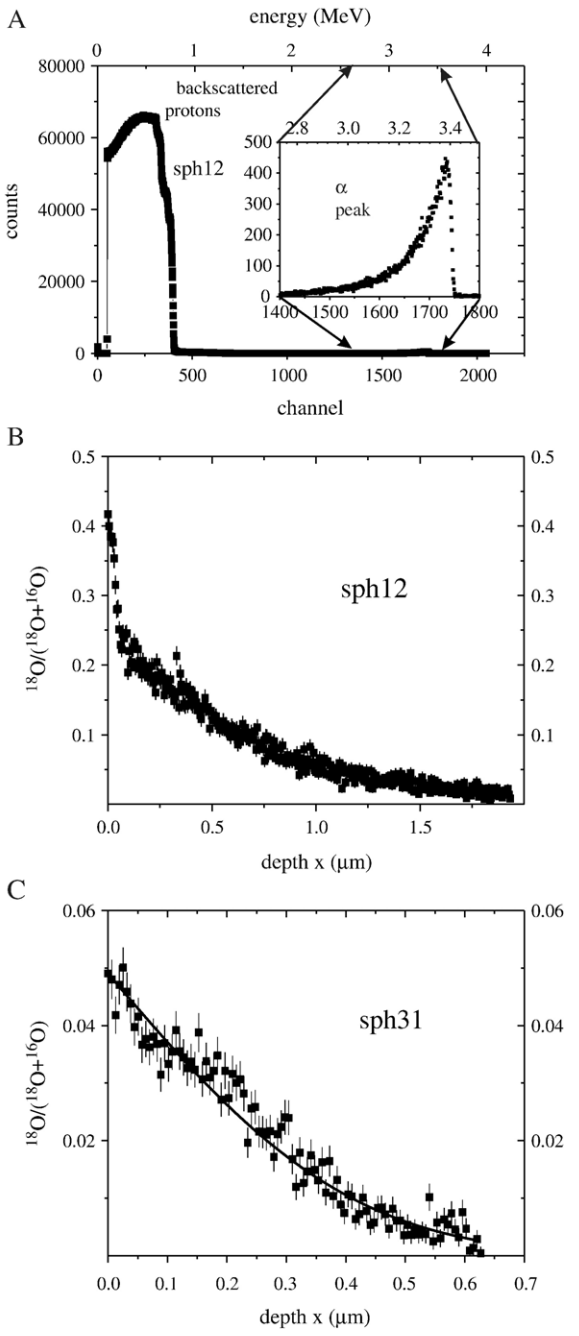

Fig. 2. A typical NRA spectrum and resulting diffusion concentration profiles calculated from the α yield. (A) A typical raw NRA spectrum of particle counts versus energy. Lower x axis is the channel number; upper x axis is the corresponding energy. The high energy (higher channel numbers) counts are α particles produced in the nuclear reaction of incident protons with ^{18}O (see enlarged area for details). The lower-energy end of the spectrum is the contribution due to backscattered protons. (B) An example of a "tailed" ^{18}O profile indicating the presence of two diffusion paths. (C) An example ^{18}O profile that fits a simple error function solution.

The oxygen diffusion profiles of euhedral synthetic titanite crystals conformed well with Eq. (1). An example profile and the linear regression from its inversion through the error function are shown in Fig. 3.

2.3.2.2. Composite profiles. All the oxygen diffusion profiles obtained from natural titanites are composite profiles. Additionally, the profiles of synthetic titanites lacking euhedral morphology are also composite profiles. As mentioned earlier, most of the composite profiles are segmented, with distinct tails, but some of the composite profiles are apparently simple diffusion profiles (detailed kinetic classification of our composite profiles will be discussed in a later part of this section).

Once it was recognized that many of our diffusion profiles had contributions from more than one diffusion path, we developed a strategy to enable independent evaluation of the governing diffusivities in these paths — i.e. lattice diffusion and fast-path diffusion. There exists no standard protocol for doing this, and any approach requires some fundamental assumptions. We based our strategy upon that developed previously by other researchers for extracting quantitative information on grain-boundary diffusion. In making this choice, we implicitly assumed that the diffusion path responsible for "long range" transport (relative to that attributable to lattice diffusion) bears some physical resemblance to grain boundaries — specifically, that the path is assumed to be slab-like in its basic geometry; i.e., of narrow width but extending in two dimensions, analogous to the intergranular medium of a polycrystal. This geometry could not be definitively confirmed (but see Zhang et al., submitted for publication), but the systematic behavior of our results suggests that it is qualitatively accurate. The essential aspects of grain boundary diffusion are best appreciated by reference to the classification scheme of Harrison (1961). The quantitative extraction of grain-boundary diffusivities is accomplished using the mathematical formulation of Whipple (1954) and Le Claire (1963).

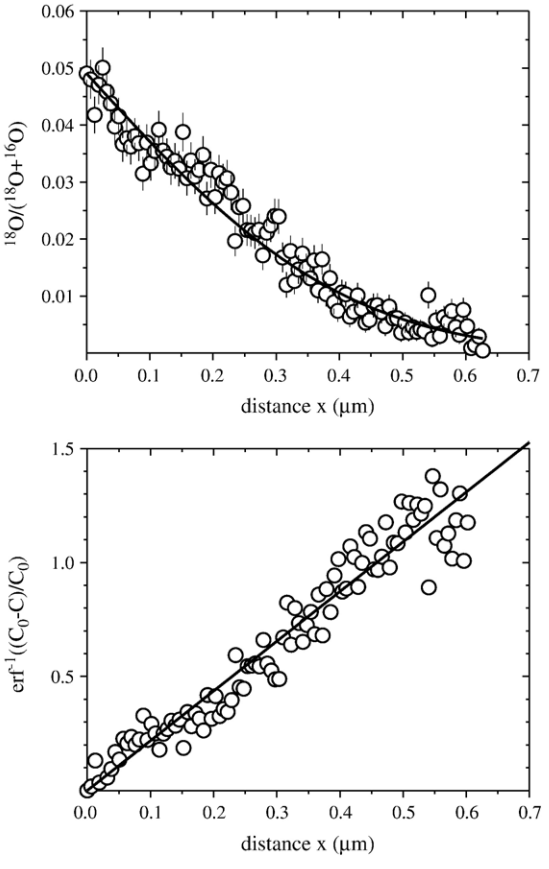

Fig. 3. A typical oxygen profile for synthetic titanite run under dry conditions. (A) The concentration data are plotted with analytical uncertainty ($\pm 1\sigma$); the smooth curve is the error function fit. (B) The same data as in (A) inverted through the error function and plotted against depth x, with linear regression line (slope$=(4Dt)^{-1/2}$).

$$\delta D_b = 1.332\sqrt{\frac{D}{t}}\left(-\frac{\partial \ln C}{\partial (z^{6/5})}\right)^{-5/3} \quad (2)$$

D_b is the diffusion coefficient in the grain boundary, D is the lattice diffusion coefficient, δ is the effective fast-path thickness, t is the annealing time, z is the depth, and C is the concentration of diffusant.

If D_f is the diffusivity in the diffusion fast path (replacing D_b with D_f), we can use the same equation to deduce the fast-path diffusivity from the tail portion of the composite diffusion profiles.

In our composite diffusion profiles, we can recognize some due to type A kinetics, some due to type B kinetics, and also some due to an intermediate type resulting from the varying magnitude of contributions from fast-path and lattice diffusion. They can be described as follows. (1) Type A profiles resemble simple error function profiles but yield larger apparent diffusivities than the expected lattice value (this was recognized only after comparison with our other experimental results); in this case the lattice diffusion fields around adjacent fast paths completely overlap. (2) Type B profiles have tails of varying size with an obvious point separating the profile into two parts, a short profile largely due to volume diffusion, and the longer tail representing the fast-path diffusion. (3) Profiles intermediate between types A and B have large tails but no obvious point of separation, as a consequence of partially overlapping diffusion fields

between adjacent fast-diffusion paths. Whether the profile can be easily recognized as exhibiting a "tail" depends on the degree of the overlap.

The Whipple-LeClaire equation is appropriate for the analysis of for the composite profiles only when these type conforms to type B diffusion kinetics in the Harrison (1961) scheme, i.e., where the diffusion fields around adjacent fast paths do not overlap. Consequently, it is only in the case of type B profiles that the diffusity for lattice diffusion (D) and δD_f can both be evaluated.

The Whipple-LeClaire equation is based on the assumption of evenly distributed parallel planar fast-diffusion paths (in polycrystals, these would be grain boundaries; in single crystals, they would be planar defects) normal to the crystal surface; it is also assumed that all the planar defects have the same thickness. Levine and MacCallum (1960) showed that the Whipple-LeClaire equation is also valid for grain boundary self-diffusion in a polycrystal containing randomly oriented grains of random size with average intergranular spacing L, and average boundary thickness δ. This model has been used to fit diffusion profiles in polycrystals in many studies (e.g., Farver and Yund, 1991b, 1998). The "tailed" diffusion profiles of our single crystals with fast-diffusion paths are similar to diffusion profiles for polycrystalline materials with grain boundaries, so it is reasonable to invoke the same model (Yurimoto et al., 1989; Yurimoto and Nagasawa, 1989; Prot and Monty, 1996; Amami et al., 1999).

Fig. 4 shows how the fast-diffusion paths contribute a tail to the diffusion profiles. It should be noted that with our analytical method, the beam spot is relatively large (about 1 mm^2), so each analysis represents an average over a large surface area of the sample likely encompassing numerous diffusional fast paths. Because the width of a fast-diffusion path is usually very small, the total amount of diffusant stored in it can be ignored. The tail is present because the diffusant moves much farther along the fast-diffusion paths than directly through the lattice. The diffusant moving through the fast paths can leave the fast-diffusion paths and diffuse into the bulk crystal on both sides of the boundaries of the fast-paths. How much diffusant enters into the bulk crystal through these fast-diffusion path depends on the time, depth and concentration difference between fast-diffusion paths and the adjacent lattice. In the fast-diffusion path, the diffusant diffuses much faster into the bulk crystal and it obeys Fick's second law. In the lattice, the diffusant moves at a relatively slow rate but also obeys Fick's second law. At a given depth, the concentration differences between the fast-diffusion path and its adjacent lattice are determined by the concentration

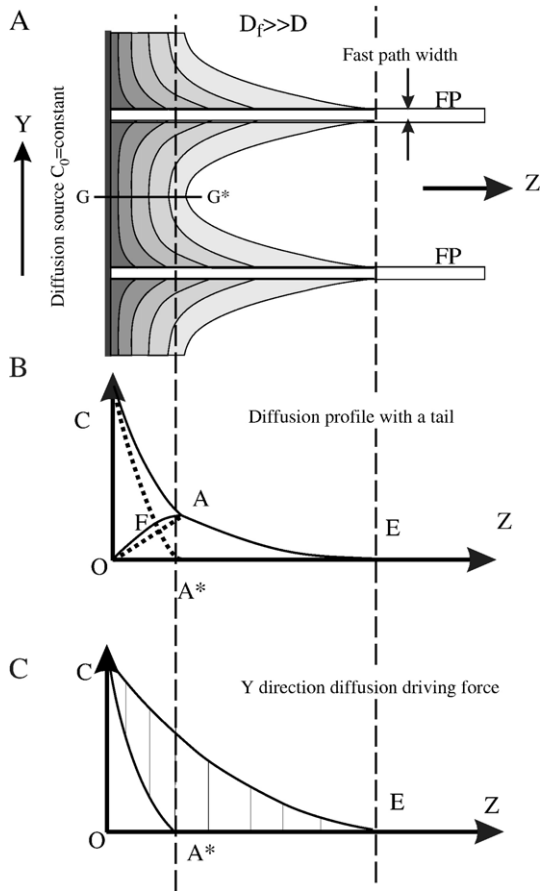

Fig. 4. Schematic diffusion concentration contours with constant surface concentration and perpendicular fast-diffusion paths, showing resulting spatially averaged concentration profiles. (A) Concentration contour of the local area near fast paths. (B) Composite diffusion profile (average over large area with many fast paths; in the actual analyses the area is ~0.1–1 mm^2). The near-surface steep part (curve CA) is due mainly to direct lattice diffusion from the surface along the Z direction, with minor contributions from the fast paths. The "tail" (curve AE) is due to fast paths only. The fast-path contribution to the overall concentration profile is represented by curve OFAE. CA* in (B) and (C) represents the contribution from direct lattice diffusion from the surface. (C) CE represents diffusion profile along the fast paths themselves (not measurable) which conforms to the error function but is also volumetrically insignificant. CA* is the diffusion profile with no fast-path contribution, e.g. along line GG* in panel (A). See text for further discussion.

difference of the above two profiles. There is no concentration difference at the surface, but it increases until it reaches its maximum value at the direct lattice diffusion front. From that point it decreases, moving further into the bulk crystal to the end of the profile in the fast-diffusion path. The overall contribution to the average concentration profile from lattice diffusion in the Y direction from a fast-diffusion path is curve OFAE. This means that we can separate out the direct lattice

diffusion profile if we can subtract curve OFAE from curve CAE. The curve OFA can only be obtained rigorously through a very complicated mathematical analysis (Kaur and Gust, 1989, p. 54) that is possible when D_f, D, δ and C_0 are well known. In the actual experiments and the data analyses, we do not know these parameters, so cannot obtain the exact curve. However, we can use the straight dashed line OA to approximate curve OFA. Using this method we obtain very consistent results for lattice diffusivities and fast-path diffusivities (see Section 3). After subtracting line OA from curve OFA, so we get a simple error function profile, and can get the lattice diffusion coefficient by the same procedure as described in Section 2.3.2.1. After obtaining the lattice diffusivity, the tail of the diffusion profile was analyzed using the Whipple-Le Claire equation.

The details of this fitting approach for a "tailed" diffusion profile, along with an example of a result are shown in Fig. 5. In the type B diffusion regime, D_f and δ cannot be evaluated independently, so all the D_f values are determined assuming $\delta = 1$ nm, following the suggestion of Atkinson et al. (1985) when comparing grain boundary diffusion and lattice diffusion data (Joesten, 1991). As most of the fast-diffusion paths are likely to be 2–3 monolayers in width, $\delta = 1$ nm is a reasonable estimate for use in evaluating D_f.

3. Results and discussion

3.1. Results

3.1.1. Dry experiments

Under dry conditions, oxygen diffusion in natural titanites appears to involve two pathways: (slow) lattice diffusion and fast-path diffusion. In the case of lattice diffusion, a least-squares fit of log$D$ vs. $1/T$ yields a pre-exponential factor of 3.03×10^{-8} m^2/s (log$D_0 = -7.52 \pm 0.74$) (the uncertainty here and throughout this paper is reported as 1σ error) and an activation energy (E_a) of

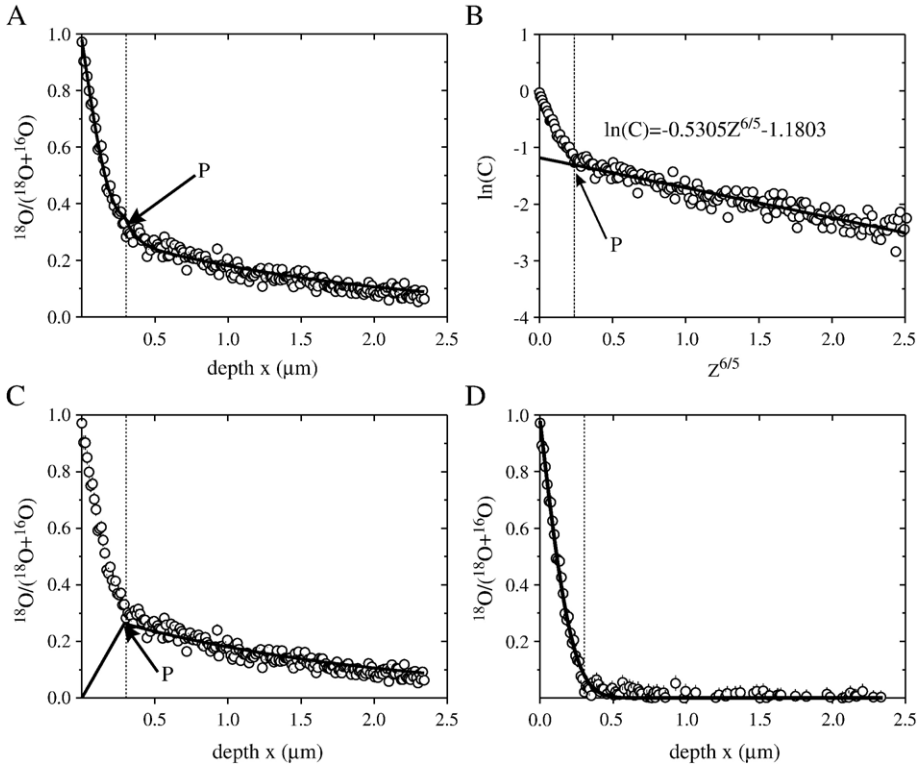

Fig. 5. Analysis of a composite diffusion profile with an obvious break in slope at P. This break can be found either by plotting ln(C) vs. $Z^{6/5}$ (as in B) or by inverting the entire profile through the error function (in which case the point of departure from a straight line would occur at P). Both methods give the same point of separation between the curve segments. (A) A composite profile and the overall fit curve. (B) Linear fit of ln(C) vs. $Z^{6/5}$ (the slope of this line gives δD_f if the lattice diffusion coefficient D is known). (C) The fast-path contribution (determined as in C) superimposed on the composite profile. Subtracting the fast-path contribution leaves the lattice diffusion contribution, which is shown in (D) with a simple error function solution fit to determine the lattice diffusion coefficient. See text for further discussion.

276±16 kJ/mol. For fast-path diffusion, the pre-exponential factor is 4.03×10^{-2} m^2/s ($\log D_0=-1.40\pm0.98$) and the activation energy is 313±22 kJ/mol.

The synthetic titanite crystals chosen for dry experiments are clear single crystals with euhedral morphology. Lattice diffusion only was observed in these diffusion profiles. These lattice diffusivities fit the same Arrhenius law as those obtained from the composite diffusion profiles of natural titanite crystals within error (Fig. 6A). A *t*-test demonstrating the equality of the fit parameters for the two sets of lattice diffusion data supports the above observations.

From the dry experiment results, we know that trace elements and fluorine content do not measurably affect the oxygen diffusion (the synthetic crystal has a higher F content than natural crystals, and different natural titanite crystals have different trace element contents). Also, we can say that our lattice diffusivity data reduction method for composite profiles (profiles with diffusion tails) appears justified. The same conclusion will also be reached for the results of wet experiments.

3.1.2. Hydrothermal experiments

Under hydrothermal conditions, oxygen diffusion in natural titanites can be attributed to a combination of lattice and fast-path diffusion using the reasoning applied to the dry case. For lattice diffusion at 100 MPa water pressure, the pre-exponential factor is 2.05×10^{-12} m^2/sec ($\log D_0=-11.69\pm1.08$) and activation energy is 180±22 kJ/mol. The fast-path Arrhenius parameters are $D_0=3.48\times10^{-7}$ m^2/s ($\log D_0=-6.46\pm1.95$) and $E_a=219\pm39$ kJ/mol.

Synthetic titanite crystals used for hydrothermal experiments were not of sufficiently high quality, and composite diffusion profiles were observed. Lattice diffusivities and fast-path diffusivities of these synthetic titanites follow the same Arrhenius relations with that of the natural titanite crystals within error (Fig. 6B).

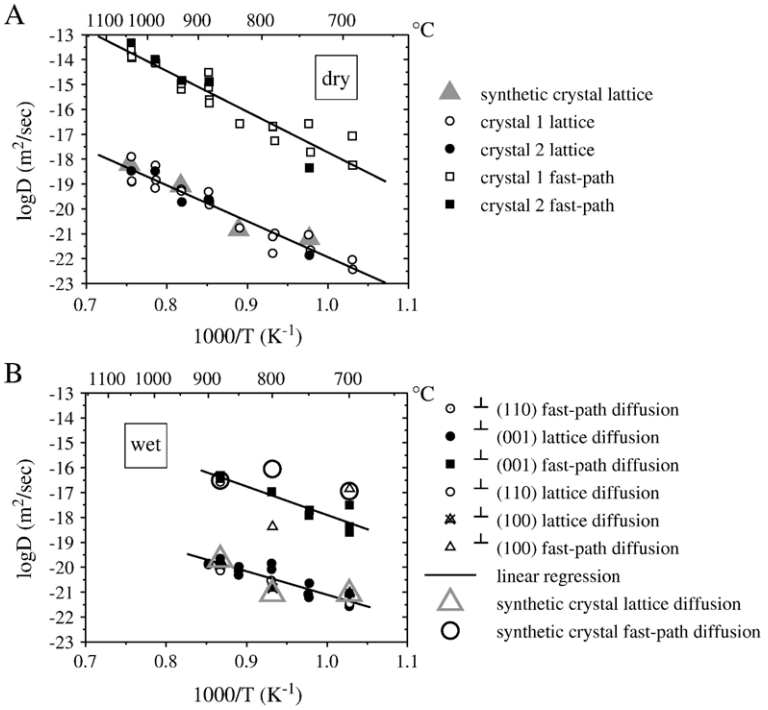

Fig. 6. Arrhenius plots for oxygen diffusion in titanite under dry (A) and hydrothermal (B) conditions. The lines are least-squares fits to each set of diffusion data. (A) From the fit to the dry lattice diffusion data an activation energy of 276±16 kJ/mol and pre-exponential factor of 3.03×10^{-8} m^2/s ($\log D_0=-7.52\pm0.74$) are obtained. From the fit to the dry fast-path diffusion data an activation energy of 313±22 kJ/mol and pre-exponential factor of 4.03×10^{-2} m^2/s ($\log D_0=-1.40\pm0.98$) are obtained. Note that different natural titanites fall along the same lines, and also that synthetic titanite from dry experiments shows only lattice diffusion, with a diffusivity falling on the lattice diffusion line for natural titanites. (B) From the hydrothermal diffusion data at 100 MPa water pressure, for lattice diffusion we obtain an activation energy of 180±22 kJ/mol and pre-exponential factor of 2.05×10^{-12} m^2/s ($\log D_0=-11.69\pm1.08$); and for fast-path diffusion, we obtain an activation energy of 219±39 kJ/mol and pre-exponential factor of 3.48×10^{-7} m^2/s ($\log D_0=-6.46\pm1.95$). Different symbols representing different crystal directions show no obvious anisotropy of oxygen diffusion.

Fig. 6B also shows that diffusion coefficients for different directions in natural titanites follow the same Arrhenius laws which indicate that there is no diffusive anisotropy.

3.1.3. Variable H_2O pressure

For our two pressure-series experiments conducted both at 800 °C (10–160 MPa water pressure) and 880 °C (10–100 MPa water pressure), respectively, there is no significant dependence of diffusivities on water pressure (Fig. 7). As in the case of zircon (Watson and Cherniak, 1997), the diffusivity of oxygen in titanites is not sensitive to changes in water pressure, but is sensitive to whether or not water is present. The presence of water reduces the activation energy of both lattice diffusion and fast-path diffusion.

The weak water pressure dependence of oxygen diffusion makes the application of these diffusion data much easier, because knowledge of specific water pressure is not necessary to apply these diffusion data. The only information necessary is whether the system is "wet" or "dry".

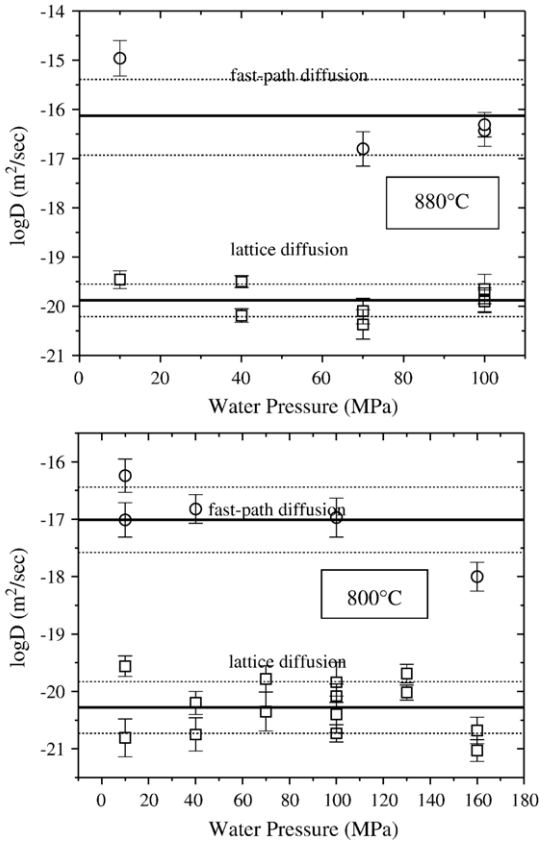

Fig. 7. Two pressure series of oxygen diffusion in titanite: at 800 °C, 10–100 MPa and at 880 °C, 10–100 MPa. No obvious pressure dependence of oxygen diffusivity in titanite was observed. The solid lines are the average value of the diffusivities and dashed lines are $\pm 2\sigma$ error range of the average value.

3.1.4. Time series

The time series for dry experiments at 900 °C is plotted in Fig. 8A, and for hydrothermal experiments at 850 °C and 100 MPa water pressure is shown in Fig. 8B. The span of run durations is almost 2 orders of magnitude, and we obtained similar diffusivities for both lattice and fast-path diffusion over the entire range.

3.2. Discussion

3.2.1. Oxygen diffusion at "dry" conditions vs. "wet" conditions

3.2.1.1. Lattice diffusion. Oxygen lattice diffusion in titanite has different Arrhenius parameters under hydrothermal conditions and under dry conditions, but the values of diffusivities themselves are very close within the 700–900 °C temperature range of this study. The slope of the Arrhenius line of "wet" diffusion is smaller than that of "dry" diffusion in titanite, which means that hydrothermal conditions lead to a reduction in the activation energy for oxygen diffusion. The activation energy under dry conditions is 276 ± 16 kJ/mol, and the activation energy under hydrothermal conditions is 180 ± 22 kJ/mol. Because these two Arrhenius lines appear close together, we did a *t*-test of the quality of the fit of these lines and the result is that the slopes are statistically different.

From the experimental results, we can see that the Arrhenius lines of wet and dry cross over at ~900 °C. Because of practical limitations in the temperature and pressure range of the experiments, we could not obtain wet diffusion data above 900 °C, consequently, we do not know wet diffusion systematics above this temperature. However, extrapolated to our diffusion data down to lower temperature, the difference between wet diffusion and dry diffusion will increase with decreasing temperature.

While comparing lattice diffusion data "wet" vs. "dry", we found that oxygen diffusion in titanite behaves in a manner similar to other minerals, i.e., oxygen diffusion under wet conditions has lower activation energy and smaller pre-exponential factor than under dry conditions. The Arrhenius line for wet diffusion thus crosses over the dry diffusion line at high temperature. For most minerals, the crossover point is much higher than the temperature range of geological interest, so water-present conditions enhance oxygen diffusion

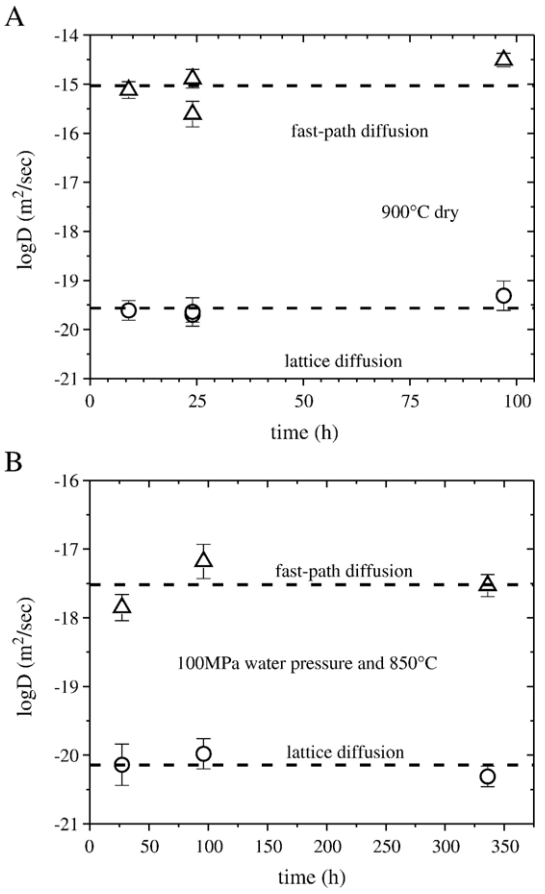

Fig. 8. Two time series – 'dry' (A) and 'wet' (B) – showing that the measured diffusivities (both lattice and fast-path) do not depend upon experiment duration. Dashed lines are the average value of the diffusivities.

significantly. Oxygen lattice diffusion behavior in a few accessory minerals (zircon, monazite and titanite) is compared in Fig. 9. In general, "wet" vs. "dry" diffusion in titanite is similar to that in the other minerals, but at temperatures of geological interest, H_2O does not enhance diffusion as markedly in the case of titanite relative to the other minerals. At 600 °C, for example, dry diffusion in zircon will be almost 7 orders of magnitude slower than "wet" diffusion; for monazite, the difference is roughly 4 orders of magnitude, and for titanite only 1.5 orders of magnitude.

The reason that water reduces the activation energy and pre-exponential factor of oxygen diffusion is still unclear. It is generally agreed that the wet diffusion is atomistically more complicated than dry diffusion. In the absence of water, oxygen atoms diffuse as lattice oxygen, probably via a vacancy mechanism. Under wet conditions, however, oxygen might diffuse as a different species, such as neutral H_2O molecules. Alternatively, the presence of H-bearing components such as water, OH^-, H_2, or H^+ in the lattice under water-present conditions can affect structural bonds, possibly resulting in reduced activation energy. If under wet conditions the diffusion mechanism is still via oxygen vacancies, incorporation of positively charged H^+(whether as hydrous groups or in some other form) will depress the concentration of oxygen vacancies, which also have an effective positive charge, thus decreasing the pre-exponential factor for the diffusing oxygen species. If a significant fraction of the diffusing oxygen species diffuses as OH^-, the pre-exponential factor would be reduced further since OH^-(in oxygen sites) and oxygen vacancies have effective positive charges and repel each other. Experiments of previous workers (Elphick and Graham, 1988; Graham and Elphick, 1991) demonstrated that the H-bearing component is not H_2 in other silicates. They suggested it might be transient protons (H^+) (Graham and Elphick, 1991). Zhang et al. (1991) have discussed the speciation of multi-component diffusion of oxygen at wet conditions based on water out-diffusion experiments on rhyolite glass with different water contents. They measured the water profile and OH^- profiles with IR spectroscopy. Through modeling the diffusion profiles, they reached the conclusion that molecular water is the fast-diffusing species, and that OH^- diffusion profiles are generated by the reaction of water with lattice O^{2-}, and argue that oxygen wet diffusion in crystals might work the same way. Assuming this argument applies to titanite, it is still difficult to link the water diffusion with the ^{18}O profile, because we do not have the ability to profile OH^- and molecular H_2O independently over the relevant depth range.

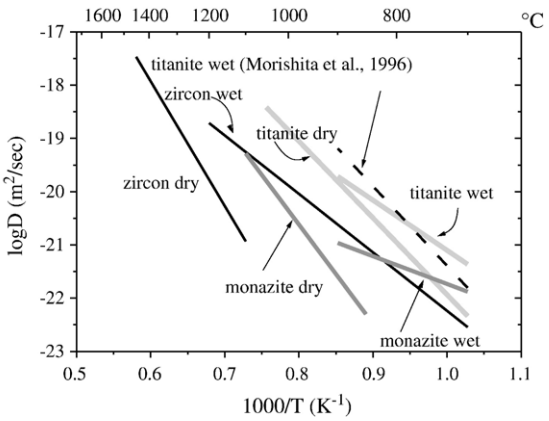

Fig. 9. Comparison of oxygen lattice diffusion in titanite with oxygen diffusion in other accessory minerals. Monazite data from Cherniak et al. (2004), zircon data from Watson and Cherniak (1997), titanite data from this study and Morishita et al. (1996).

3.2.1.2. Fast-path diffusion. The presence of water appears to reduce the activation energy for fast-path diffusion only slightly, but the statistically different Arrhenius slopes mean that at low temperature the "wet" diffusivity will slightly surpass the "dry" diffusivity. At 600 °C, for example, the "wet" fast diffusivity is about a factor of 4 times faster than the "dry" fast diffusivity—a marginally significant difference given the uncertainties in slopes. The activation energy under dry conditions is 313±22 kJ/mol, and the activation energy under hydrothermal conditions is 219±39 kJ/mol. Because these two Arrhenius lines are close together, we did a *t*-test of the quality of the fit of these lines and the result is that the slopes are different statistically. The presence of water likely reduces the activation energy by the same mechanisms that operate in the case of lattice diffusion.

3.2.2. Lattice diffusion vs. fast-path diffusion

Under dry conditions, the fast-path diffusivity is about 5 orders of magnitude larger than that for lattice diffusion; under wet conditions, the fast-path diffusion is about 4 orders of magnitude faster (Fig. 6). It is easy to imagine why diffusion along fast paths outpaces diffusion through the lattice, but it is much less clear why the diffusion difference between lattice and fast paths is 5 orders of magnitude in dry conditions but 4 orders of magnitude in wet conditions. In general – whatever the exact nature of the fast paths – the lattice is probably discontinuous across them, creating relatively large molecular "voids" through which oxygen (or H_2O) can move through more freely. This is analogous to the case of a low-angle grain boundary, but it should be emphasized that the observed fast paths are obviously not grain boundaries but are more likely a two-dimensional lattice defect. We have no explanation to offer for the decreased difference between the lattice and fast-path diffusivities under wet conditions.

For dry conditions, fast-path diffusion has an activation energy of 313±22 kJ/mol, which is slightly higher than the lattice diffusion activation energy of 276±16 kJ/mol; however, the uncertainties make these values essentially indistinguishable. Similarly, for wet conditions, fast-path diffusion has an activation energy of 219±39 kJ/mol which is slightly higher than the lattice diffusion activation energy of 180±22 kJ/mol, but again, because of the uncertainties, we can say that they are in agreement.

The increase in diffusion rate along grain boundaries is usually linked to a decrease in activation energy (Farver and Yund, 1991b, 1998; Nogueira et al., 2003). There are, however, a few opposite examples, e.g., oxygen diffusion in Cr_2O_3 polycrystals (activation energy for lattice diffusion 280 kJ/mol, for grain boundary diffusion 675 kJ/mol Sabioni et al., 1992a,b,c) and oxygen diffusion in macroperthitic feldspar (the activation energy for grain-boundary diffusion is 179 kJ/mol and for lattice diffusion it is 108 kJ/mol, respectively; Nagy and Giletti, 1986). Sabioni et al. (1992c) argued that impurity segregation is responsible for the increase of the activation energy for oxygen diffusion in grain boundaries within the Cr_2O_3 polycrystals. No evidence supporting this argument has yet been found.

It would seem logical to expect that oxygen diffusion along the fast paths in single crystals has a lower activation energy than that for the oxygen lattice diffusion. However, only a few opposite observations have been made that show the activation energy for fast-path diffusion is higher than the activation energy of lattice diffusion, e.g., oxygen and aluminum diffusion in alumina single crystals (Le Gall and Lesage, 1994; Prot and Monty, 1996; Prot et al., 1996; Le Gall et al., 1996) and oxygen diffusion in single crystal melilite (Yurimoto et al., 1989). In the Prot et al. (1996) paper, a similar argument was pointing to that the impurity (yttrium) segregation as the cause of the higher grain boundary activation energy for oxygen diffusion in Al_2O_3 polycrystals. These authors further extended the argument to the case of fast paths. As in the case of grain boundaries, clear evidence to support the argument is lacking.

However, it should be stressed that the titanite data do not make a compelling case for large differences in activation energy either one way or the other between lattice and fast-path diffusion of oxygen.

3.2.3. Comparison with cation diffusion in titanite

Data exist for diffusion of other elements in titanite, including several of geochronological and geochemical interest (Sr, Nd, Pb and Zr). Sr diffusion data can be used to understand Sr isotope ratios measured in titanite; Nd diffusion can be used to understand Sm–Nd age retention as well as REE zoning and systematics in titanite. Lead diffusion can be used to evaluate the mobility of Pb isotopes and interpret U–Th–Pb ages. Zr diffusion data could be used to evaluate the potential thermometer of Zr in titanite. The oxygen diffusion data reported in this study could be used to interpret the measured oxygen isotope ratios in titanites, which could be applied in understanding thermal histories or determining the likelihood of retentivity of original oxygen isotope signatures in mineral grains.

A summary Arrhenius plot of diffusion in titanite is presented in Fig. 10. From the comparison of the

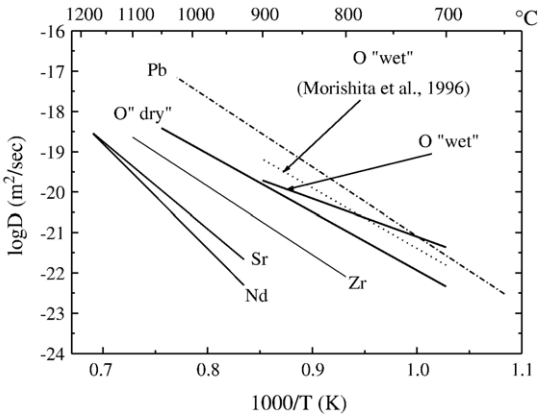

Fig. 10. Summary Arrhenius plots of lattice diffusion of cations and oxygen in titanite. Sr and Nd data are from Cherniak (1995), Pb from Cherniak (1993), Zr from Cherniak, submitted for publication, oxygen data from this study and Morishita et al. (1996). See text for details.

diffusion rates, the following conclusions can be reached:

(1) In titanite, oxygen diffuses much faster than the REE. Oxygen isotope ratios measured might represent later events than the REE signature does, as oxygen isotopes are more likely altered by diffusion than are the REE.
(2) The diffusivities of lead and oxygen are very similar, so in many cases measured oxygen isotope ratios in titanite may be linked to the U–Pb age, provided both O and Pb isotopes are altered only by lattice diffusion.

4. Geochemical implications

Diffusion data are often used to understand radioisotope dating, cooling, thermometry of trace element partitioning, thermometry of isotope partitioning, and zoning structure in some minerals. Our new oxygen diffusion data for titanite can be used to interpret the oxygen isotope measurements made on titanite grains (to determine whether or not the original isotope signature could be preserved in a particular grain or a region of a grain), to assess retention in the mineral cores and in rims if there is zoning, and to evaluate isotope partitioning thermometry in mineral pairs including titanite.

In this section, we will apply our lattice diffusion data in discussing two aspects of oxygen isotopes in titanite. Although our experimental results showed that rapid diffusion paths do exist in natural titanite crystals, these rapid paths are probably isolated from one other on the scale of mineral grains, so they may account for only a small percentage of oxygen transport under most circumstances.

The experimental measurements are of ^{18}O diffusion specifically ($^{18}O \leftrightarrow {}^{16}O$ exchange), but when we talk about oxygen isotope signatures measured in mineral grains, we use $\delta^{18}O$, a modified $^{18}O/^{16}O$ ratio. In a diffusion profile, however, the $^{18}O/^{16}O$ concentration ratios will vary with depth not exactly as a simple error function (as separate measurements of ^{18}O and ^{16}O profiles would), but as the ratio of two quantities, each with a distinct error function relationship. However, since the natural abundance of ^{18}O is 0.204%, $^{18}O/^{16}O$ is almost equal to $^{18}O/(^{18}O+{}^{16}O)$, so the value of $^{18}O/^{16}O$ as a function of time and depth does actually closely conform to an error function since the denominator is effectively constant. Therefore, we can treat the ratio $^{18}O/^{16}O$ as having the same diffusivity as ^{18}O, and use the ^{18}O diffusivity to discuss the retentivity of $\delta^{18}O$ (Watson and Cherniak, 1997). We can also use the ratio in discussing general questions of bulk closure or specific considerations of oxygen isotope retention in mineral cores or rims, even though the actual diffusants are ^{18}O and ^{16}O, not the $^{18}O/^{16}O$ ratio or the $\delta^{18}O$ value.

4.1. Bulk closure temperature

For all of the questions we will consider, the key is whether or not the system of interest will be reset by diffusion under P–T conditions different from those under which the initial $\delta^{18}O$ was acquired. For cooling scenarios, the bulk closure temperature is usually used as a criterion because no significant diffusive loss or gain is considered to occur below it. As a theoretical concept the meaning of closure temperature is clear, but in actual systems many factors affect the actual bulk close temperature, including peak temperature, cooling rate, diffusion parameters (activation energy and pre-exponential factor), grain size, and mode of mineral constituents (Eiler et al., 1992).

The equation most often used to calculate the cooling closure temperature was developed by Dodson (1973, 1986):

$$T_c = \frac{E/R}{\ln \frac{ART_c^2(D_0/a^2)}{E(\mathrm{d}T/\mathrm{d}t)}} \quad (3)$$

where T_c is Dodson's cooling closure temperature, E is the activation energy for diffusion, R is gas constant, D_0 is pre-exponential factor of the diffusion, a is the effective diffusion radius (often assumed to be the radius of the grain), $\mathrm{d}T/\mathrm{d}t$ is the cooling rate, and A is geometric factor (55 for a sphere).

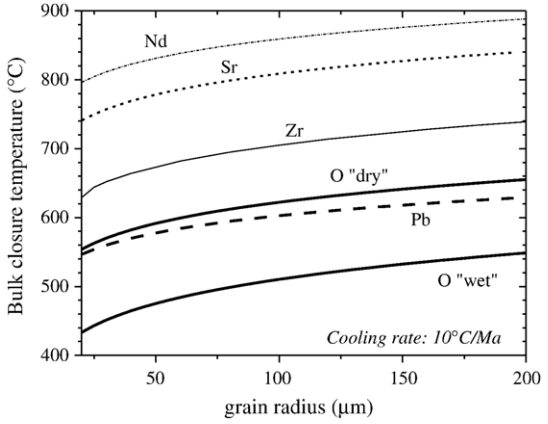

Fig. 11. Dodson's cooling closure temperature for oxygen in titanite, under both "dry" and "wet" conditions. The Dodson cooling closure temperatures for Pb, Zr, Sr and Nd are also plotted for comparison. Calculations are based on diffusion parameters: Sr, Nd diffusion from Cherniak (1995), Pb diffusion from Cherniak (1993) and Zr from Cherniak, submitted for publication.

Two assumptions are important in Dodson's derivation: (1) there is an infinite reservoir of the element of interest in the environment surrounding the mineral grains, and constant concentration of this element is maintained; (2) the initial (peak) temperature is high, with diffusion fast and cooling slow. These conditions ensure that the system starts cooling as a completely open system, so that the closure temperature is not dependent on the initial temperature which is the condition $\{RT^2D_{t=0}/(E(\mathrm{d}T/\mathrm{d}t)a^2) \gg 1$, which must be satisfied to validate Dodson's bulk closure temperature equation.

When assumption (2) is unjustified but assumption (1) is still valid, Dodson's bulk closure temperature concept cannot be used. Since the system is not completely open at the initial temperature, the composition at the center of the grain is not completely reset, so the closure temperature recorded in the grain is dependent on the initial temperature. Ganguly and Tirone (1999) discussed the closure temperature under these conditions, and provided methods to calculate closure temperature for the conditions $0<M\leq 1.2$ as a modification to Dodson's equation, they definite $M=RT^2D_{t=0}/(E(\mathrm{d}T/\mathrm{d}t)a^2)$. From their results, when $M<10^{-2}$, at the initial temperature, the system is already completely closed.

For accessory minerals, assumption (1) is generally justified because accessory minerals only account for a very small portion of the mineral components consisting of the rocks and their diffusion loss or gain will have negligible effects on their environment. In general discussion and comparisons, Dodson's closure temperature can still be used to give a general idea of accessory mineral behavior as long as reasonable cooling rates apply. When discussing accessory minerals in specific rocks, however, the peak temperature usually does affect the recorded closure temperature. In principle, if at the peak temperature the system is not completely open, the closure temperature recorded (weighted average closure profile) is lower than the closure temperature cooling from a completely open system. Because closure temperature is higher in a grain center than in its rim, the center of a grain in a partially open system has the initial temperature

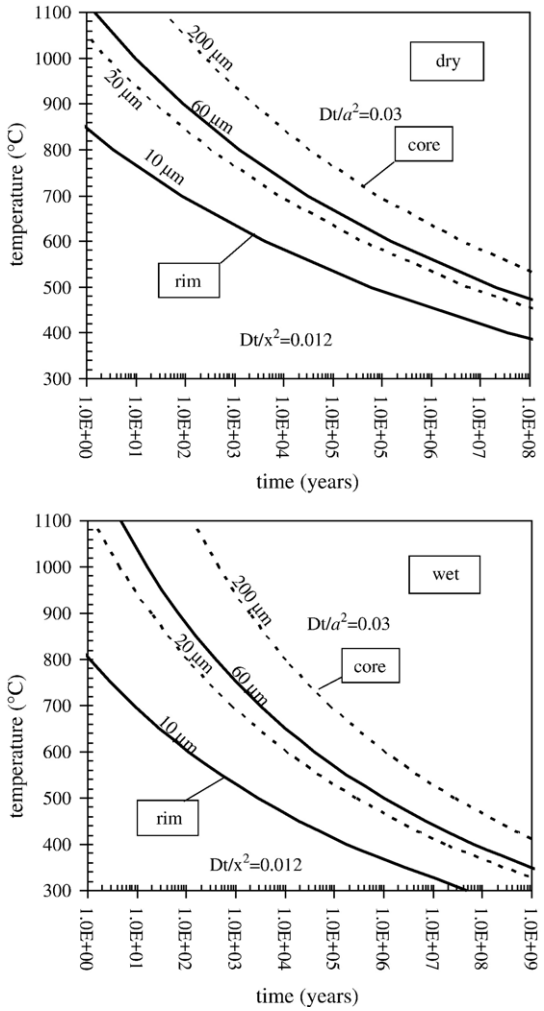

Fig. 12. Oxygen isotope center-retention upper time limit for isothermal annealing of titanite cores and rims under both wet and dry conditions. The curves are the maximum anneal duration at specific temperature that a spherical core or rim can experience and still remain its original oxygen isotope ratio at the center. The maximum time was calculated by center-retention criteria: $Dt/a^2=0.03$ for core and $Dt/x^2=0.012$ ("a" and "x" are radius of core and thickness of rim, respectively).

recorded as the closure temperature which is lower than the closure temperatures if cooling from an open system. Accordingly, the weighted average closure temperature will also be lower.

For oxygen diffusion in titanite, for the size range 20–200 μm, we calculated the effects of initial cooling temperature to closure temperature using Ganguly and Tirone (1999) method. We found that at cooling rate 10 °C/Ma, for the above mentioned size range, at dry conditions for peak tempertures as low as 700 °C and at wet conditions for peak tempertures as low as 600 °C their method still gives the same closure temperature as Dodson's equation.

In Fig. 11, we show the comparison of Dodson's closure temperatures in titanite from 20 μm to 200 μm grain sizes, calculated for Pb, Nd, Sr, and oxygen, using Eq. (3) and spherical geometry. It is immediately clear that Sr and Nd close at much higher temperatures than Pb and oxygen. Pb closure temperatures are close to oxygen "dry" values, and slightly higher than oxygen "wet" values. In dry systems, the oxygen isotope signature preserved could be linked to Pb isotopic dates, but for wet systems, this might not be the case. In addition, REE signatures in titanite are much more resistant to diffusive loss than oxygen, under either wet or dry conditions.

4.2. Retention at rim and core center during isothermal events

The zoning of REEs, Y, Al and Fe has been noted in titanite (Paterson and Stephens, 1992; Frost et al., 1999; Piccoli et al., 2000). If zoning of oxygen isotopes accompanied these chemical differences, the question of whether the distinct $\delta^{18}O$ signature would be preserved becomes important. Although present technology cannot measure $\delta^{18}O$ at the same depth resolution as our measurements of ^{18}O diffusion profiles, the ability to measure oxygen isotope ratios in situ with small beam spots (Valley and Graham, 1991, 1993) still allows us to explore the internal oxygen isotopic structure to some extent, at least in examining potential oxygen isotopic differences between the rim and the core of titanite grains.

With the titanite diffusivity data, we can calculate and make predictions about the time limit that we can expect oxygen isotope retentivity in a crystal core or rim. To make the boundary conditions simple, we assume a two step concentration distribution in the titanite grain (this is not necessarily true in nature, but it simplifies discussion and calculations). The mineral core is modeled as a sphere, with one initial ^{18}O concentration, and the rim a hollow sphere with a different initial ^{18}O concentration. It is assumed that the ^{18}O concentration at the sphere surface maintains a constant value during the isothermal annealing. The $^{18}O/^{16}O$ "center retention" criterion for a sphere of radius "a" will be $Dt/a^2 \leq 0.03$ (Crank, 1967, p.86). For the rim, the relevant model is that for a hollow sphere. If we assume the same constant $^{18}O/^{16}O$ ratio was maintained at both the inner and outer surface of this hollow sphere, we can use the solution of Crank (1967, p.94) to derive the center retention criterion, for $b/a = 0.1–2$ (b is the outer radius of the rim, a is the radius of the core), which covers the core/rim dimensions of interest. We obtain the criterion of $Dt/x^2 \leq 0.012$ for retention near the mid-point of a rim of thickness x (i.e., $b-a$). It should be noted that the same constant-surface condition will not generally be met at the inner boundary (due to the presence of the core and the effects of the radial dilution effect). As long as the initial oxygen $^{18}O/^{16}O$ is retained at the center of the rim, i.e., the inward and outward diffusion fields do not meet—the above approximation gives sufficient accuracy.

In Fig. 12, on the temperature vs. time plot, the limitting curves for center retention of $^{18}O/^{16}O$ in titanite cores ($Dt/a^2 = 0.03$) and rims ($Dt/x^2 = 0.012$) are illustrated for diffusion loss or gain under both dry and hydrothermal conditions. At high lower-crust temperatures (~800 °C), 200 μm radius titanite cores will retain their original $^{18}O/^{16}O$ ratios for about 9000 or 34 800 years, for wet and dry conditions, respectively. Rims of 20 μm thickness will retain their original $^{18}O/^{16}O$ rim ratios for about 4 or 14 years, for wet or dry conditions, respectively. At typical mid-crust metamorphic temperatures (~500 °C), 200 μm radius titanite cores will retain original $^{18}O/^{16}O$ ratios for about 2.7 Ma or 570 Ma, for wet and dry conditions, respectively. Rims of 20 μm thickness will retain original $^{18}O/^{16}O$ ratios for about 1.1 Ma or 2.4Ma, for wet and dry conditions, respectively.

From the above calculations, it can be concluded that titanite will not retain its original igneous oxygen isotope signature through high-grade metamorphism. In general, diffusion will reset the oxygen isotope signatures, even though the mineral itself can survive the event.

Acknowledgments

We thank Dr. James Van Orman for his thorough review of the manuscript. This research was supported by NSF through the grant EAR-0073752 and EAR-0440228 to Dr. E.B. Watson.

References

Amami, B., Addou, M., Millots, F., Sabiono, A., Monty, C., 1999. Self diffusion in α-Fe_2O_3 natural single crystals. Ionics 5, 358–370.

Atkinson, A., Pummery, F.C.W., Monty, C., 1985. Diffusion of ^{18}O tracer in NiO grain boundaries. In: Sinkiovich, G., Stubican, V.S. (Eds.), Transport in Nonstoichiometric Compounds, NATO ASI Series. Series B. Physics, vol. 129, pp. 1071–1091.

Cherniak, D.J., 1990. A particle-accelerator based study of major and trace element diffusion in minerals. Ph.D. Dissertation, State University of New York at Albany, Albany N.Y., 219 pp.

Cherniak, D.J., Watson, E.B., 2001. Pb diffusion in zircon. Chemical Geology 172, 5–24.

Cherniak, D.J., Contributions to Minerology and Petrology. Zr diffusion in titanite(sphene) (submitted for publication).

Cherniak, D.J., Zhang, X.Y., Nakamura, M., Watson, E.B., 2004. Oxygen diffusion in monazite. Earth and Planetary Science Letters 226, 161–174.

Choudhury, A., Palmer, D.W., Amsel, G., Curien, H., Baruch, P., 1965. Study of oxygen diffusion in quartz using the nuclear reaction ^{18}O (p,α) ^{15}N. Solid State Communications 3, 119–122.

Coghlan, R.A.N., 1990. Studies on diffusional transport of oxygen in feldspars, strontium and the REEs in garnet, and the thermal histories of granitic intrusions in south-central Maine using oxygen isotopes. Ph.D. Dissertation, Brown University, Providence, 237 pp.

Cole, D.R., Chakraborty, S., 2001. Rate and mechanisms of isotopic exchange. In: Valley, J.W., Cole, D.R. (Eds.), Stable Isotope Geochemistry. Reviews in Mineralogy and Geochemistry, vol. 43. Mineralogical Society of America, pp. 83–223.

Crank, J., 1967. The Mathematics of Diffusion. Oxford University Press, New York. 347 pp.

Dennis, P.F., 1984. Oxygen self-diffusion in quartz under hydrothermal conditions. Journal of Geophysical Research B 89, 4039–4046.

Derdau, D., Freer, R., Wright, K., 1998. Oxygen diffusion in anhydrous sanidine feldspar. Contributions to Mineralogy and Petrology 133, 199–204.

Dodson, M.H., 1973. Closure temperature in cooling geochronogical and petrological systems. Contributions to Mineralogy and Petrology 40, 259–274.

Dodson, M.H., 1986. Closure profiles in cooling systems. Materials Science Forum 7, 145–154.

Eiler, J.M., Baumgartner, L.P., Valley, J.W., 1992. Intercrystalline stable isotope diffusion: a fast grain boundary model. Contributions to Mineralogy and Petrology 112, 543–557.

Elphick, S.C., Graham, C.M., 1988. The effect of hydrogen on oxygen diffusion in quartz: Evidence for fast proton transients? Nature 335, 243–245.

Elsenheimer, D., Valley, J.W., 1991. In situ oxygen isotope analysis of silicates; a tale of two lasers. Abstracts with Programs-Geological Society of America 23, 262.

Elsenheimer, D., Valley, J.W., 1992. In situ oxygen isotope analysis of feldspar and quartz by Nd: YAG laser microprobe. Chemical Geology 101, 21–42.

Farver, J.R., 1989. Oxygen self-diffusion in diopside with application to cooling rate determinations. Earth and Planetary Science Letters 92, 386–396.

Farver, J.R., 1994. Oxygen self-diffusion in calcite: dependence on temperature and water fugacity. Earth and Planetary Science Letters 121, 575–587.

Farver, J.R., Giletti, B.J., 1989. Oxygen diffusion in amphiboles. Geochimica et Cosmochimica Acta 49, 1403–1411.

Farver, J.R., Yund, R.A., 1991a. Oxygen diffusion in quartz: dependence on temperature and water fugacity. Chemical Geology 90, 55–70.

Farver, J.R., Yund, R.A., 1991b. Measurement of oxygen grain boundary diffusion in natural, fine-grained, quartz aggregates. Geochimica et Cosmochimica Acta 55, 1597–1607.

Farver, J.R., Yund, R.A., 1998. Oxygen grain boundary diffusion in natural and hot-pressed calcite aggregates. Earth and Planetary Science Letters 161, 189–200.

Fortier, S.M., Giletti, B.J., 1991. Volume self-diffusion of oxygen in biotite, muscovite, and phlogopite micas. Geochimica et Cosmochimica Acta 55, 1319–1330.

Frost, B.R., Chamberlain, K.R., Schumacher, J.C., 2001. Sphene (titanite): phase relations and role as a geochronometer. Chemical Geology 172, 131–148.

Frost, C.D., Frost, B.R., Chamberlain, K.R., Edwards, B.R., 1999. Petrogensis of the 1.43G Sherman batholith, SE Wyoming: a reduced rapakivi-type anorogenic granite. Journal of Petrology 40, 1771–1802.

Ganguly, J., Tirone, M., 1999. Diffusion closure temperature and age of a mineral with arbitrary extent of diffusion: theoretical formulation and applications. Earth and Planetary Science Letters 170, 131–140.

Gerard, O., Jaoul, O., 1989. Oxygen diffusion in San Carlos Olivine. Journal of Geophysical Research B 94, 4119–4128.

Giletti, B.J., Hess, K.C., 1988. Oxygen diffusion in magnetite. Earth and Planetary Science Letters 89, 115–122.

Gilletti, B.J., Yund, R.A., 1984. Oxygen diffusion in quartz. Journal of Geophysical Research 89, 4030–4046.

Giletti, B.J., Semet, M.P., Yund, R.A., 1978. Studies in diffusion: III. Oxygen diffusion in feldspars: an ion microprobe determination. Geochimica et Cosmochimica Acta 42, 45–57.

Graham, C.M., Elphick, S.C., 1991. Some experimental constraints on the role of hydrogen in oxygen and hydrogen diffusion and Al–Si interdiffusion in silicates. In: Ganguly, J. (Ed.), Diffusion, Atomic Ordering, and Mass Transport — selected Topics in Geochemistry. Advances in Physical Geochemistry, vol. 8. Springer-Verlag Press, pp. 248–285.

Harrison, L.G., 1961. Influence of dislocation on diffusion kinetics in solids with particular reference to alkali halides. Transactions of the Faraday Society 57, 1191–1199.

Jaoul, O., Froidevaux, C., Durham, W.B., Michaut, M., 1980. Oxygen self-diffusion in forsterite: implications for the high-temperature creep mechanism. Earth and Planetary Science Letters 47, 391–397.

Jaoul, O., Houlier, B., Abel, F., 1983. Study of ^{18}O diffusion in magnesium orthosilicate by nuclear microanalysis. Journal of Geophysical Research 88, 613–624.

Joesten, R., 1991. Grain boundary diffusion kinetics in silicate and oxide minerals. In: Ganguly, J. (Ed.), Diffusion, Atomic Ordering, and Mass Transport-Selected Topics in Geochemistry. Advances in Physical Geochemistry, vol. 8. Springer-Verlag press, pp. 345–395.

Kaur, I., Gust, W., 1989. Fundamentals of Grain and Interphase Boundary Diffusion, Second Revised Edition. Ziegler Press, Stuttgart. 422 pp.

King, E.M., Valley, J.W., Davis, D.W., Kowallis, B.J., 2001. Empirical determination of oxygen isotope fractionation factors for titanite with respect to zircon and quartz. Geochimica et Cosmochimica Acta 65, 3165–3175.

Kowallis, B.J., Christiansen, E.H., Griff en, D.T., 1997. Compositional variations in titanite. Abstracts with Programs—Geological Society of America 29, 402.

Le Claire, A.D., 1963. The analysis of grain boundary diffusion measurements. Journal of Applied Physics 14, 351–356.

Le Gall, M., Lesage, B., 1994. Self-diffusion in α-Al_2O_3: I. Aluminum diffusion in single crystals. Philosophical Magazine A 70, 761–773.

Le Gall, M., Huntz, A.M., Lesage, B., 1996. Self-diffusion in α-Al_2O_3: III. Oxygen diffusion in single crystals doped with Y_2O_3. Philosophical Magazine A 73, 919–934.

Levine, H.S., MacCallum, C.J., 1960. Grain boundary and lattice diffusion in polycrystalline bodies. Journal of Applied Physics 31, 595–599.

Mojzsis, S.J., Harrison, T.M., Pidgeon, R.T., 2001. Oxygen-isotope evidence from ancient zircons for liquid water at the earth's surface 4,300 Myr ago. Nature 409, 178–181.

Moore, D.K., Cherniak, D.J., Watson, E.B., 1998. Oxygen diffusion in rutile from 750 to 1000 °C and 0.1 to 100 MPa. American Mineralogist 83, 700–711.

Morishita, Y., Giletti, B.J., Farver, J.R., 1996. Volume s elf-diffusion of oxygen in titanite. Geochemical Journal 30, 71–79.

Nagy, K.L., Giletti, B.J., 1986. Grain boundary diffusion of oxygen in a macroperthitic feldspar. Geochimica et Cosmochimica Acta 50, 1151–1158.

Nogueira, M.A.N., Ferraz, W.B., Sabioni, A.C.S., 2003. Diffusion of the ^{65}Zn radiotracer in ZnO polycrystalline ceramics. Materials Research 6, 167–171.

Pacaud, L., Ingrin, J., Jaoul, O., 1999. High temperature diffusion of oxygen in synthetic diopside measured by nuclear reaction analysis. Mineralogical Magazine 63, 673–686.

Paterson, B.A., Stephens, W.E., 1992. Kinetically induced compositional zoning in titanite: implications for accessory-phase/melting partitioning of trace elements. Contributions to Mineralogy and Petrology 109, 285–373.

Peck, W.H., Valley, J.W., Wilde, S.A., Graham, C.M., 2001. Oxygen isotope ratios and rare earth elements in 3.3 to 4.4 Ga zircons: Ion microprobe evidence for high $\delta^{18}O$ continental crust and oceans in the early Archean. Geochimica et Cosmochimica Acta 65, 4215–4229.

Piccoli, P., Candela, P., Rivers, M., 2000. Interpreting magmatic processes from accessory phases: titanite-a small-scale recorder of large-scale processes. Transactions of the Royal Society of Edingbergh: Earth Sciences 9, 257-257.

Prot, D., Monty, C., 1996. Self-diffusion in α-Al_2O_3: II. Oxygen diffusion in "undoped" single crystals. Philosophical Magazine A 73, 899–917.

Prot, D., Le Gall, M., Lesage, B., huntz, A.M., Monty, C., 1996. Self-diffusion in δ-Al_2O_3: IV. Oxygen grain boundary self-diffusion in undoped and yttria-doped alumina polycrystals. Philosophical Magazine A 73, 935–949.

Reddy, K.P.R., Cooper, A.R., 1982. Oxygen diffusion in sapphire. Journal of American Ceramics Society 65, 634–638.

Robin, R., Cooper, A.R., Heuer, A.H., 1973. Application of a nondestructive single-spectrum proton activation technique to study oxygen diffusion in zinc oxide. Journal of Applied Physics 44, 3770–3777.

Ryerson, F.J., Durham, W.B., Cherniak, D.J., Lanford, W.A., 1989. Oxygen diffusion in olivine: Effect of oxygen fugacity and implications for creep. Journal of Geophysical Research 94, 4105–4118.

Sabioni, A.C.S., Lesage, B., Huntz, A.M., et al., 1992a. Self-diffusion in Cr_2O_3: 1. Chromium diffusion in single-crystals. Philosophical Magazine A 66, 333–350.

Sabioni, A.C.S., Huntz, A.M., Millot, F., et al., 1992b. Self-diffusion in Cr_2O_3: 2. Oxygen diffusion in single-crystals. Philosophical Magazine A 66, 351–360.

Sabioni, A.C.S., Huntz, A.M., Millot, F., et al., 1992c. Self-diffusion in Cr_2O_3: 3. Chromium and oxygen grain boundary diffusion in polycrystals. Philosophical Magazine A 66, 361–374.

Valley, J.W., Graham, C.M., 1991. Ion microprobe analysis of oxygen isotope ratios in granulite facies magnetites: Diffusion exchanges as a guide to cooling history. Contribution to Mineralogy and Petrology 109, 38–52.

Valley, J.W., Graham, C.M., 1993. Cryptic grain-scale heterogeneity of oxygen isotope ratios in metamorphic magnetite. Sciences 259, 1729–1733.

Valley, J.W., Chiarenzelli, J.R., McLelland, J.M., 1994. Oxygen isotope geochemistry of zircon. Earth and Planetary Science Letters 126, 187–206.

Watson, E.B., Cherniak, D.J., 1997. Oxygen diffusion in zircon. Earth and Planetary Science Letters 148, 527–544.

Whipple, R.T.P., 1954. Concentration contours in grain boundary diffusion. Philosophical Magazine 45, 1225–1236.

Wiechert, U., Hoefs, J., 1995. An excimer laser-based micro analytical preparation technique for in-situ oxygen isotope analysis of silicate and oxide minerals. Geochimica et Cosmochimica Acta 59, 4093–4101.

Wiechert, U., Fiebig, J., Przybilla, R., Xiao, Y., Hoefs, J., 2002. Excimer laser isotope-ratio-monitoring mass spectrometry for in situ oxygen isotope analysis. Chemical Geology 182, 179–194.

Wilde, W.H., Valley, J.W., Peck, W.H., Graham, C.M., 2001. Evidence from detrital zircons for the existence of continental crust and oceans on the earth 4.4 Gyr ago. Nature 409, 175–178.

Yau, L.C., Peacor, D.R., Essene, E.J., 1987. Authigenic anatase and titanite in shale from the Salton Sea Geothermal Field, California. Neues Jahrbuch für Mineralogie Abhandlungen 10, 441–452.

Yurimoto, H., Nagasawa, H., 1989. The analysis of dislocation pipe radius for diffusion. Mineralogical Journal 14, 171–178.

Yurimoto, H., Morioka, M., Nagasawa, H., 1989. Diffusion in single crystals of melilite: I. Oxygen. Geochimica et Cosmochimica Acta 53, 2387–2394.

Zhang, Y., Stolper, E.M., Wasserburg, G.J., 1991. Diffusion of a multi-species component and its role in oxygen and water transport in silicates. Earth and Planetary Science Letters 103, 228–240.

Zhang, X.Y., Watson, E.B., Cherniak, D.J., submitted for publication. Oxygen self-diffusion "fast-paths" in titanite single crystals and a general method for deconvoluting self-diffusion profiles with "tails". Geochimica et Cosmochimica Acta.